Classification of Alzheimers Disease using RF Signals and Machine Learning

Classification of Alzheimer's Disease using RF Signals and Machine Learning

Imran M. Saied, Tughrul Arslan, *Senior Member, IEEE*, and Siddharthan Chandran

Abstract: **Objectives:** Alzheimer's disease is one of the most fastest growing and costly diseases in the world today. It affects the livelihood of not just patients, but those who take care of them, including care givers, nurses, and close family members. Current progression monitoring techniques are based on MRI and PET scans which are inconvenient for patients to use. In addition, more intelligent and efficient methods are needed to predict what the current stage of the disease is and strategies on how to slow down its progress over time. **Technology or Method:** In this paper, machine learning was used with S-parameter data obtained from 6 antennas that were placed around the head to noninvasively capture changes in the brain in the presence of Alzheimer's disease pathology. Measurements were conducted for 9 different human models that varied in head sizes. The data was processed in several machine learning algorithms. Each algorithm's prediction and accuracy score were generated and the results were compared to determine which machine learning algorithm could be used to efficiently classify different stages of Alzheimer's disease. **Results:** Results from the study showed that overall, the logistic regression model had the best accuracy of 98.97% and efficiency in differentiating between 4 different stages of Alzheimer's disease. **Clinical or Biological Impact:** The results obtained here provide a transformative approach to clinics and monitoring systems where machine learning can be integrated with noninvasive microwave medical sensors and systems to intelligently predict the stage of Alzheimer's disease in the brain.

Keywords **— Machine Learning, RF, Alzheimer's disease, predictive diagnostics, Microwave medical diagnostics**

I. Introduction

ALZHEIMER'S disease (AD) is quickly becoming a global challenge that is affecting not just elderly people, but their caregivers, nurses, and close family members close. With the current rapid increase in the ageing population, AD is also becoming not only a fast-growing disease, in terms of the number of people affected, but an even faster, larger, and costlier burden to society that imposes a social and economic threat for the next 30 to 40 years [1]. In addition, the disruption in ongoing care and research for AD due to ongoing pandemic is likely to impact and increase these numbers [2].

It is therefore of paramount importance to investigate, develop, and deploy solutions to intelligently, quickly, and noninvasively detect and monitor the progression of AD in patients. This will enable doctors and caregivers to predict the course of the disease and determine which treatment strategies are effective. Machine learning (ML) techniques combined with advanced sensing technology is an important field to provide contributions in the automatic prediction, monitoring, and early detection of AD progression.

ML has been used in the past decade to detect certain biomarkers in MRI scans for AD. Many ML methods are currently utilised to improve the determination and prediction of AD. In [3], a proof-of-concept personalized classifier for AD dementia and mild cognitive impairment (MCI) patients was presented based on biomarkers provided from [4]–[6]. In [7], precise categorisation of stable MCI versus progressive MCI was achieved by analysing 35 cases of normal controls and 67 cases of MCI with a support vector machine (SVM) [7]. Segmentation has been emphasised in most ML processes for bio-image classification, whereas the retrieval of strong texture descriptions has generally been neglected [8]. A review of several SVM-based research showed that SVM is a widely utilised method to distinguish between AD cases and cognitively normal cases and between stable forms and progressive forms of MCI [9].

Microwave sensing and imaging for medical diagnostics has developed into a lucrative area of research for several decades, due to its non-ionising technology and ability to develop devices and sensors that are portable and wearable. This technology has been used extensively in the detection of breast cancer, stroke, and most recently, neurodegenerative diseases [10]-[12]. Recently, ML has been utilised to efficiently process the captured RF signals from such devices and classify different diseases in the heart and breast using received RF signals [13],[14].

I. M. Saied and T. Arslan are with the School of Engineering, University of Edinburgh, Edinburgh, EH9 3JF UK (e-mails: Imran.Saied@ed.ac.uk & T.Arslan@ed.ac.uk).

S. Chandran is with the Centre for Clinical Brain Sciences, University of Edinburgh, Edinburgh EH9 3JF UK (e-mail: Siddharthan.Chandran@ed.ac.uk).

TABLE I
FOUR-POLE COLE-COLE MODEL PARAMETERS ACROSS 0.2 TO 3 GHZ [19]

Tissue Type	ε_∞	$\Delta\varepsilon_1$	τ_1 (s)	α_1	$\Delta\varepsilon_2$	τ_2 (s)	α_2	$\Delta\varepsilon_3$	τ_3 (s)	α_3	$\Delta\varepsilon_4$	τ_4 (s)	α_4	σ_s
Gray Matter -AD	40.12	30.09	1.73e-8	0.9903	20.06	7.98e-9	0.9942	30.09	1.73e-8	0.9903	20.06	7.98e-9	0.9942	1.23e-17
Gray Matter -Healthy	34.56	34.53	1.28e-2	0.7747	34.53	1.28e-2	0.7747	34.53	1.28e-2	0.7747	34.53	1.28e-2	0.7747	1.64e-17
White Matter -AD	12.77	6.383	4.35e-14	0.9221	6.383	4.36e-14	0.9221	6.383	4.38e-14	0.9221	6.383	4.40e-14	0.9221	2.91e-18
White Matter -Healthy	22.35	12.35	3.95e-14	0.6606	12.35	3.87e-14	0.6608	0.661	3.71e-14	0.6611	12.35	3.79e-14	0.6611	4.86e-18

Although there are no studies that investigate ML with RF data for AD detection, there have been recent studies that utilised this approach to classify stroke in the brain [15]-[17]. In [15] support vector machine (SVM) classifier is used with simulation data to detect the presence of stroke in the brain. While the use of SVM made the overall performance of the system to be more effective, the algorithm still needs to be validated with experimental data. Authors in [16] investigated 5 different ML algorithms, SVM, K-Nearest Neighbours (KNN), linear discriminant analysis (LDA), Naïve-Bayes (NB), and classification trees, to classify the presence of ischemic versus hemorrhagic stroke using experimental data. It was found that SVM and LDA algorithms had the best accuracy in differentiating ischemic and hemorrhagic stroke, while KNN had the fastest learning and classification time. However, while the study is promising, a limitation of the study is the lack of data that will help in training the algorithms better. Finally, a recent paper [17] presented a novel graph degree mutual information (GDMI) approach along with SVM in order to identify between ischemic and hemorrhagic stroke. The algorithm could obtain an accuracy of 88% and obtain results in under a minute. Although the algorithm is promising, it requires further validation on experimental data to verify its effectiveness.

While the amount of research interest in ML for classifying AD is increasing over the past decade, the majority of the focus lies on training and predicting image data from MRI and PET scans, rather than on raw signals or datasets, such as electroencephalogram (EEG) signals or radiofrequency (RF) signals. Conducting MRI and PET scans on AD patients can be inconvenient, difficult, uncomfortable, and sometimes invasive. The authors have investigated a noninvasive technique of detecting and imaging AD in the brain using reflected RF signals that are captured by wearable antennas acting as sensors [19]. This paper aims to build upon the previous work by investigating and applying ML algorithms to the captured RF signals in order to predict and classify the current stage of AD. The study conducted in this paper, to the authors' knowledge, has not been done before, and serves as a novel and transformative validation of ML techniques with RF data for medical diagnostic and predictive analytics.

II. RF DATASET BACKGROUND

In [18], the authors conducted an initial investigation of dielectric measurements of brain tissue samples obtained from two patients with severe AD. Dielectric properties were captured from tissues with and without hallmarks of AD (i.e. having amyloid-beta plaques and tau tangles). The study conducted in [18] was expanded further in [19] to perform dielectric measurements on a larger number of brain tissue samples obtained from a recently deceased patient with severe AD. This was to ensure that the effect of the sample's decay after death on the dielectric measurements was minimized. Dielectric measurements were taken between 200 MHz and 3 GHz with an Agilent high-temperature dielectric probe 85070E-0020 that was connected to the VNA (HP8753C).

While both [18] and [19] were limited in obtaining samples from a large number of people with AD, the results obtained were promising and consistent in the two studies. In particular, the relative permittivity in both the gray matter and white matter regions decreased by up to 20.86 and 19.48% respectively, while the loss factor increased by almost 17% in the gray matter and up to 44% for the white matter region. This change in the dielectric properties can be associated with the presence of AD-related plaques and tangles in the brain, which have been found to affect the transfer of essential nutrients and water to the brain [1]. This collective change in the brain's composition of nutrients and water, as a result of AD pathology, is what essentially causes the dielectric properties to change.

Based on these measurements, a four-pole Cole-Cole model ($\varepsilon_C(\omega)$) was generated in [19] as:

$$\varepsilon_C(\omega) = \varepsilon_\infty + \sum_{i=1}^{4} \frac{\Delta\varepsilon_i}{1 + (j\omega\tau_i)^{1-\alpha_i}} + \frac{\sigma_s}{j\omega\varepsilon_0} \quad (1)$$

where τ_i is the relaxation time, α_i is the exponent describing the dispersion regions, and σ_s is the static conductivity. The magnitude of the dispersion is represented by $\Delta\varepsilon_i = \varepsilon_{si} - \varepsilon_\infty$, where ε_{si} is the static permittivity when $\tau_i \ll 1/\omega$, and ε_∞ is the infinite permittivity when $\tau_i \gg 1/\omega$. The parameters of the four-

pole Cole-Cole model for each measurement is shown in Table I.

With these dielectric properties, several computational models could be created that emulated the 3 main stages of AD in a patient as mentioned by Braak in [20] (i.e., Mild AD, Moderate AD, and Severe AD). RF antennas were placed around the head to measure the reflected signals at different parts of the brain. These reflected signals, known as reflection coefficients (or S_{11}) is what is measured and recorded in the RF dataset. This study focuses on collecting RF signals for each AD stage for 9 head sizes in order to have a larger and more varied dataset of reflected RF signals.

A. Development of Models for Different Stages of Alzheimer's Disease

As mentioned earlier, after obtaining dielectric measurements, several computational models were developed in CST Microwave Studio Suite. As a starting point, a realistic human head voxel model, initially reported in [21], was used and modified in CST and shown in Fig. 1. The head model contains intricate geometries and materials that were defined to represent different regions, layers, tissues, and ventricles that are present in the brain. This model also had the advantage of being able to modify properties of specific areas or tissues. The model proved to be useful in particular for defining certain areas of the brain that contain plaques and tangles during different stages of Alzheimer's disease.

Each stage of AD was represented by changing the dielectric properties of certain regions and tissues to match those obtained from the dielectric measurements as reported in [19]. Table II lists the regions of the brain that were affected by AD in each stage and the corresponding dataset that was used. Some of the cases required both the gray matter and white matter regions to be changed as both sets of tissues were found to be affected by AD as shown by Braak in [20].

Fig. 2 (a)-(d) shows the 4 cases that were used in this study: Normal, Mild AD, Moderate AD, and Severe AD, respectively. Each of these models were developed based on the progression and location of amyloid-beta plaques and tau tangles in the brain as a result of AD as presented by Braak in [20]. Along with the head model that was obtained from [21], 8 different CST voxel models were used in the simulations that collectively make up the CST Voxel Family as described in [22] - [24] and shown in Fig. 3. Note that the Hugo model is listed as part of the Visible Human Model Dataset [23].

These models represent realistic and varied head sizes belonging to both male and female models. In order to recreate the stages of AD in each of the 8 additional head models, first the inner brain objects were deleted from the voxel model. Next, the geometries and objects of the brain from [21] (see Fig. 1) were copied and placed inside each of the head model in CST. The next step requires the copied objects and geometries to be adjusted and modified, such that they occupy the inner space of the head models. This is done using the bending features in CST. Namely, there is a tool called Bend Shape that allows each shape to bend and attach itself to another object.

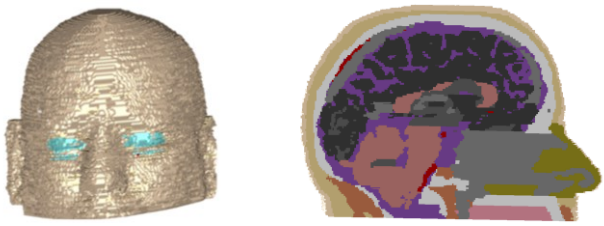

(a) (b)

Fig. 1. (a) Realistic human head model used for simulations in CST, and (b) cross-sectional view of the human head model showing the different layers, tissues and geometries of the brain.

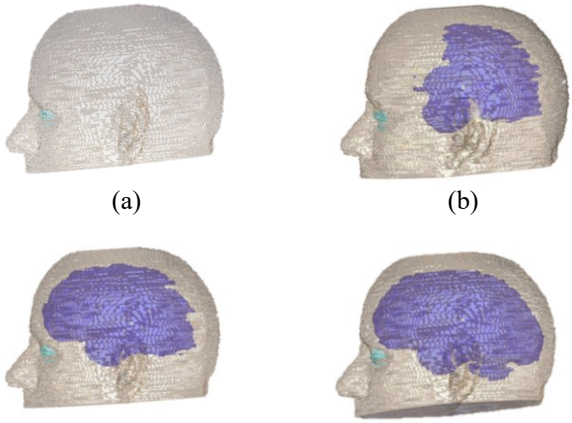

(a) (b) (c) (d)

Fig. 2. Simulation models showing the amount of AD-affected brain tissues (highlighted in blue) for the following stages of AD: (a) Normal, (b) Mild AD, (c) Moderate AD, and (d) Severe AD.

TABLE II
REGIONS OF HEAD MODEL USED FOR STAGES OF ALZHEIMER'S DISEASE

Stage	Brain Region Affected	Dielectric Property Used
Normal	None	None
Mild AD	Medial Temporal Lobe	AD White
	Temporal Lobe	AD White and AD Gray
	Parietal Lobe	AD White and AD Gray
Moderate AD	Medial Temporal Lobe	AD White
	Temporal Lobe	AD White and AD Gray
	Parietal Lobe	AD White and AD Gray
	Frontal Lobe	AD White and AD Gray
Severe AD	Medial Temporal Lobe	AD White
	Temporal Lobe	AD White and AD Gray
	Parietal Lobe	AD White and AD Gray
	Frontal Lobe	AD White and AD Gray
	Occipital Lobe	AD White and AD Gray

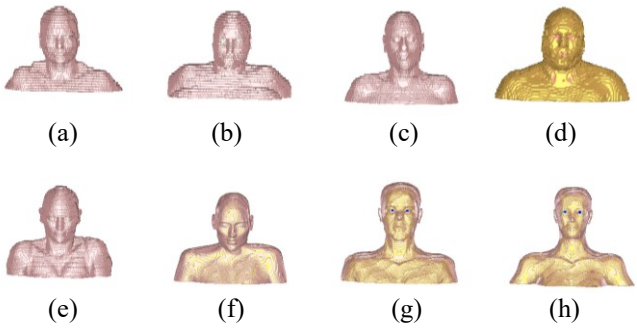

(a) (b) (c) (d)

(e) (f) (g) (h)

Fig. 3. CST models of a) Donna, b) Emma, c) Gustav, d) Hugo, e) Laura, f) Katja, g) Tom, and h) Ana that were used to capture RF data. These models are from the CST Voxel Family in CST 2020 [24].

TABLE III
PERCENTAGE OF CHANGED DIELECTRIC PROPERTIES FOR HEAD MODELS

	# of Meshcells (Brain)	Normal	Mild AD	Mod. AD	Severe AD
Head Model [21]	25,465,789	0%	55.4%	87.3%	96.4%
Donna	26,501,962	0%	57.3%	89.1%	96.8%
Emma	27,467,395	0%	56.3%	88.9%	97.5%
Gustav	24,987,435	0%	56.7%	87.1%	96.2%
Hugo	26,501,962	0%	55.9%	86.8%	95.2%
Laura	23,869,401	0%	58.1%	88.4%	97.3%
Katja	23,004,875	0%	54.3%	89.2%	98.4%
Tom	25,650,372	0%	54.7%	86.8%	95.9%
Ana	24,743,018	0%	56.2%	87.0%	96.8%

For this simulation, the brain object in [21] that was used contained 5 different layers, where each layer was made up of several sub-objects or geometries that correlated to ventricles, arteries, and other parts of the brain. Each layer was selected one at a time, starting with the outermost layer. Once the layer was selected in CST, we would select the Bend Shape tool and select the area where the object would need to be placed, which, in this case, would be the inner side of the now empty head models that were used. All the layers and objects of the copied brain model were able to conform to the inner shape of each of the 8 head models accordingly. Then, for each head model, different stages of AD were created using the same method used to alter the dielectric properties as described earlier and shown in Table II. There was a total of 36 simulation cases that were developed in CST and used in this study.

Table III shows the number of meshcells that were used for the brain for each head model, and the percentage of meshcells that had its dielectric properties altered for each case accordingly. While each model would now have the same layers, objects, and geometries as the original model in Fig. 1, some of the objects either expanded or contracted depending on the shape of the head. This had an effect on the overall number of meshcells used in the CST model for the brain, as well as the number of cells that were changed in the model when altering the region's dielectric properties for each stage of AD, as shown in Table III. Nonetheless, this provided a more realistic design approach to represent people with different head sizes, and therefore, different brain geometries. RF signals were then obtained at each antenna collectively stored into a single dataset for each simulation case.

B. RF Data Measurement

In order to obtain data, several RF antennas were designed and placed around the outer circumference of the head models. The antennas were ultrawideband (UWB) antennas, with an operating frequency range of 1.3 to 4.2 GHz. The antenna models are shown in Fig. 4.

A 0.1-mm-thick flexible conductive textile, Shieldex Zell acted as the conducting material, while the substrate is made of RS-PRO Viscose Wool Felt material with a measured relative permittivity, ε_r and loss tangent, $tan\,\delta$ of 1.55 and 0.068, respectively. The antenna is fed with a microstrip line that transitions into a stepped monopole structure in order to enhance its performance. To simultaneously improve the directionality and the bandwidth of the antenna, three rectangular shaped patches of different sizes were incorporated into the design. More details of the antennas are provided in our previous work in [19] along with dimensions of the antenna.

In RF sensing, the presence of an anomaly inside the head can be detected by changes in the dielectric properties that is reflected in the reflection coefficient of the RF waves received by the antenna. To obtain the RF dataset, 6 RF sensors were placed around each of the 9 head models and used to capture the reflection coefficient (S_{11}) for each area of the brain as shown in Fig. 5. This was done for each case (i.e. Normal, Mild AD, Moderate AD, and Severe AD). S_{11} data for each antenna was captured and stored as a single complete dataset for each case.

There were a total of 1001 points for each antenna measurement. Therefore, each simulation case contained a total of 6006 data points, or 1001 datapoints for each of the 6 antennas, between the frequency range of 0.01 to 5 GHz. Overall, the RF dataset for all the head models and their corresponding cases contained 216,216 data points. This dataset was arranged in a matrix with dimension 36×6007. Each row represents the simulation case. Each of the 6006 columns represents the antenna measurement, while the last column contains the list of classes representing the stage of AD where the measurements were taken.

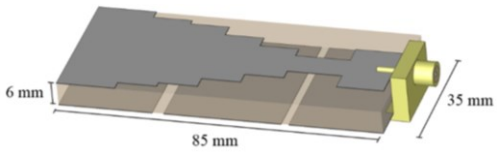

Fig. 4. Geometry of the RF textile antenna used in the simulations.

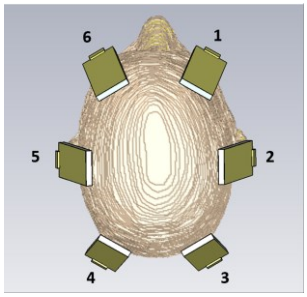

Fig. 5. Simulation model setup showing the 6 RF antennas placed around the realistic head model in CST.

III. Evaluation Methodology and Results

A. Validation of Machine Learning Algorithms

In order to efficiently develop and execute programs for machine learning, a Python environment was used in this study along with SciPy, which is an ecosystem of Python libraries such as NumPy (work with data in arrays), Matplotlib (create 2D plots), and Pandas (tools to organize and analyze data). In addition, the scikit-learn library was also used to provide tools to perform machine learning algorithms in Python and evaluate models. Specifically, the following ML algorithms were used: 1) Logistic Regression (LR) [25], 2) Linear Discriminant Analysis (LDA) [26], 3) K-Nearest Neighbours (KNN) [27], 4) Classification and Regression Trees (CART) [28], 5) Gaussian Naïve Bayes (GNB) [27], and 6) Support Vector Machines (SVM) [29].

Initially, statistical analysis was done on the RF dataset. The mean, standard deviation, min, max, and count for each antenna is shown in Table IV. The values of S_{11} are all within the same range and therefore no normalization or data scaling step needs to be done to finetune the data further. Fig. 6 shows the box plot of the dataset for each antenna in the different groups (i.e., Normal, Mild AD, Moderate AD, and Severe AD). The box plots provide a quick visualization on the distribution and spread of the datapoints for each antenna. It can be concluded from the plots that there is no clear linear or normal distribution of data for each antenna. This provides the assumption that ML algorithms based on Gaussian or normal distribution (e.g. GNB), may not work well with this RF dataset.

To extend this visualization and analysis further, a scatter plot matrix was also generated and shown in Fig. 7 to show the relationship between each of the antennas' data with each other. Two important trends can be distinguished from Fig. 7.

TABLE IV
Statistical Analysis on RF Dataset

	Ant. 1	Ant. 2	Ant. 3	Ant. 4	Ant. 5	Ant. 6
Count	36036	36036	36036	36036	36036	36036
Mean (dB)	-17.78	-6.818	-3.021	-9.598	-7.877	-3.84
Std. Dev. (dB)	8.50	3.41	1.39	8.29	4.89	1.41
Min (dB)	-109.4	-38.22	-20.19	-90.56	-43.99	-18.89
Max (dB)	-1.49	-1.74	-1.74	-1.11	-1.76	-0.99

First, all antenna measurements were not found to be highly correlated with each other, which suggests that there are differences between antennas' data that makes one independent from the other.

This finding indicates the possibility that ML algorithms, like LR and LDA, will have a better performance for this dataset, whereas algorithms like KNN and SVM would have a poor performance from such a dataset. It should be noted that the KNN algorithm is based on the distance between features of the new observation and training data. As a result, this algorithm is more susceptible to data corruption if new observations are very similar to those in the training dataset. Another important finding from Fig. 7 is that the histogram plots for each antennas' data shows an exponential distribution that validates the box plots shown in Fig. 6, where the antennas' data is not normally distributed. This important finding also provides an additional assumption to ML algorithms, like GNB, which will not perform well on the given RF dataset.

In the next phase, 6 different machine learning algorithms were evaluated on the RF dataset. Later, statistical methods were used to estimate the accuracy of the models on unseen data. In addition, a more concrete method was needed to estimate the accuracy of the best model by evaluating it on data separate validation dataset. Specifically, some data from the RF dataset will be held back so that the algorithms will not get biased during its training phase. This method will provide a second and independent idea of how accurate the best model might actually be.

To accomplish this, first the RF dataset was split into two sets; 28 complete simulation cases (approximately 78%) were used to train the models (e.g. training dataset) and the remaining 8 simulation cases (approximately 22%) were used as the validation dataset. This split was done randomly by using a random number generator in Python to randomly select rows of the dataset and extract its complete datapoints to store in the validation dataset array.

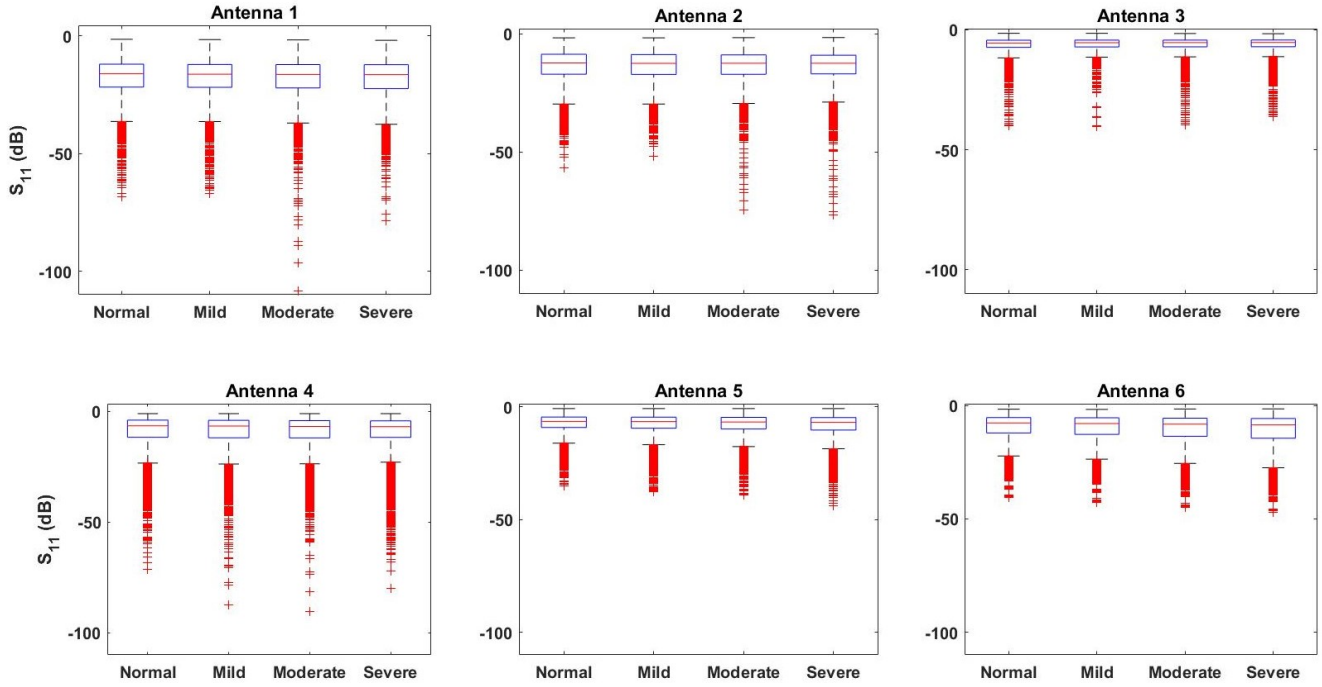

Fig. 6. Box plot showing distribution of data for each antenna amongst the different test cases (Normal, Mild AD, Moderate AD, and Severe AD). It can be noted that the data does not appear to be normally distributed in the plots.

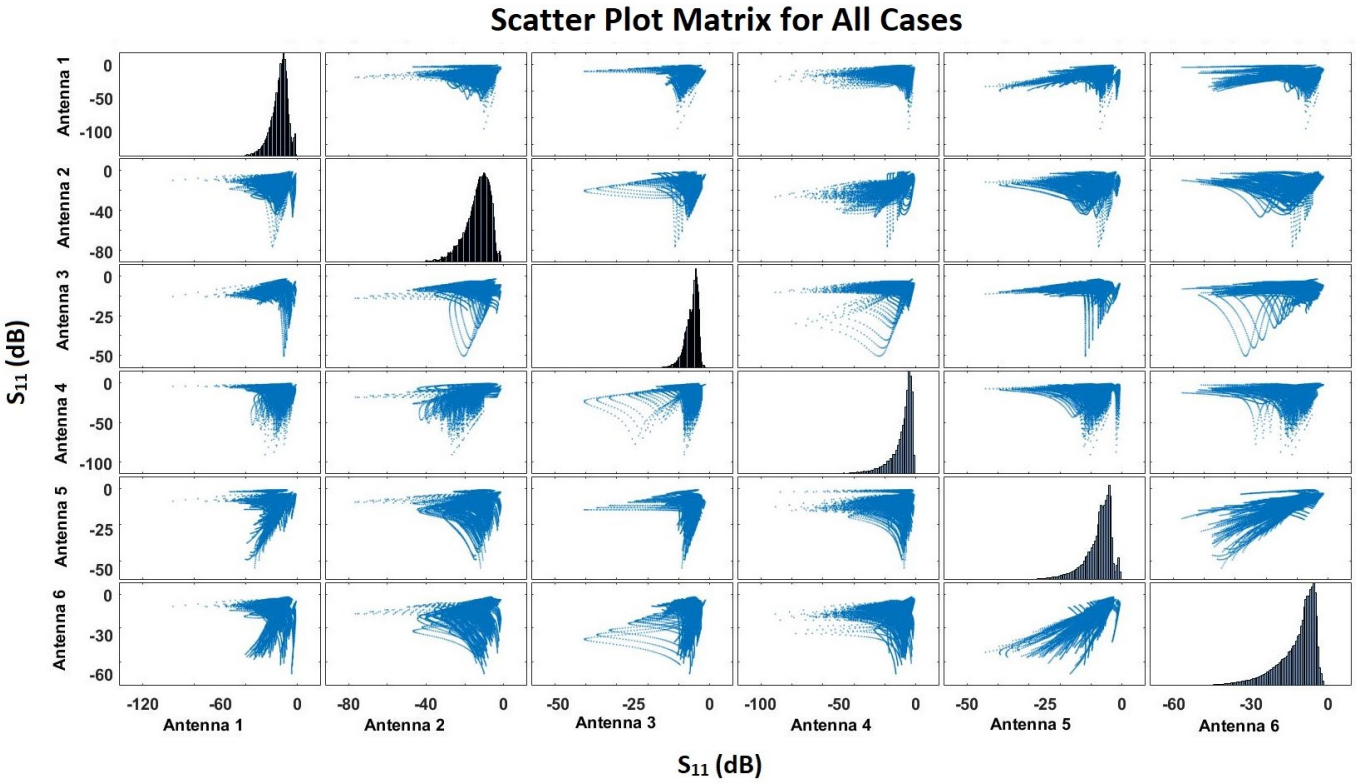

Fig. 7. Scatter plot matrix showing the relationship of each antenna's data with other antennas for all cases. The diagonal plots show the histogram of datapoints for each antenna. It is noted that the histograms show that the data is exponentially distributed for each antenna.

The next step is to setup a test harness that will use k-fold cross validation to estimate accuracy of the models on the training dataset. In this step, the dataset is first shuffled randomly, and split into k groups. One unique group is taken out and held as a test dataset, while the remaining groups are used as a training dataset. A model is fitted on

TABLE V

AVERAGE MEASURED ACCURACY FOR EACH MODEL

Algorithms	Accuracy (%)	Std. Dev.
LR	98.965	0.001
LDA	95.5647	0.001234
KNN	58.00	0.3023
CART	78.667	0.06182
GNB	43.3333	0.2348
SVM	21.333	0.1222

the training set and evaluated it on the test dataset. An evaluation score is then generated and used to summarise the skill of the model. The value of k must be chosen carefully for the dataset. There is no formal rule, but as k gets larger, the difference in size between the training set and the resampling subsets gets smaller. As this difference decreases, the bias of the technique becomes smaller [30].

Typically, given these considerations, one performs k-fold cross-validation using k = 5 or k = 10, as these values have been shown empirically to yield test error rate estimates that suffer neither from excessively high bias nor from very high variance [31]. Therefore, we have used k=10 in our model. This will split the dataset into 10 parts, train on 9 and test on 1, and repeat for all combinations of train-test splits. The resulting accuracy metric is used to evaluate the models. This is a ratio of the number of correctly predicted instances divided by the total number of instances in the dataset (e.g. a value of 0.95 corresponds to 95% accuracy). This scoring variable will then be used when running, building, and evaluating each model.

The final step is to build the machine learning models for the RF dataset. 6 different ML algorithms were evaluated: LR, LDA, KNN, CART, GNB, and SVM. This list is a good mixture of simple linear (LR and LDA) and nonlinear (KNN, CART, NB and SVM) ML algorithms. A random number seed is reset before each run to ensure that the evaluation of each algorithm is performed using exactly the same data splits. This ensures that the results are directly comparable. The ML algorithms were evaluated 10 times in Python. After running each model on the dataset, the accuracy estimations were calculated and stored. After the 10^{th} iteration, the accuracy estimations for each model were averaged and shown in Table V. In addition, a box plot shown in Fig. 8 was generated to compare the distribution of the recorded accuracy estimations for each model.

Most of the algorithms had accuracy levels below 80%, except for LR and LDA. LR in particular has the highest estimated average accuracy score of 98.97%, while LDA had an estimated average accuracy of 0.9556 or 95.56%. This could be due to the uncorrelated relationship amongst the antennas' data, which makes it easier for the LR and LDA algorithms to focus on independent features that differ between the cases.

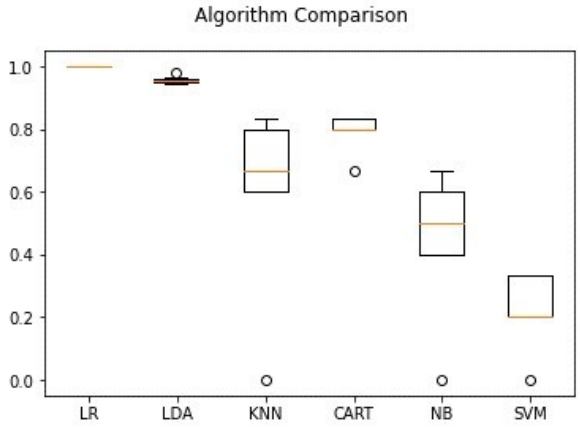

Fig. 8. Box plot comparing the distribution of estimated accuracy values for each algorithm.

The poor performance of KNN, CART, GNB, and SVM were all alluded to by the plots in Figs. 6 and 7 that showed the data distribution and relationships of the RF dataset. Therefore, it was expected that most of these algorithms would not perform well with the RF dataset.

B. Evaluating LR Algorithm with Validation Dataset

The LR algorithm's high accuracy provided an incentive to carry out further validation. Another test was conducted on the accuracy of the model, but this time using the validation dataset. By performing another test on the model using a validation dataset, we can eliminate factors such as overfitting or data leak that would make this model overly optimistic in its prediction. After running the model with the validation dataset, the final accuracy was calculated as 100% (i.e., the LR model could accurately distinguish all the cases successfully). In addition, Tables VI and VII below show the confusion matrix and classification report of the 4 main classes in this dataset (Normal, Mild AD, Moderate AD, and Severe AD).

It can be seen in Table VI that the true positives (e.g. Normal-Normal, Mild AD-Mild AD, etc., that are located in the diagonal of the table) far outweigh the other prediction errors outside the diagonal. This shows that the trained LR ML model performs very well in predicting and labelling the current stage of AD based on new RF data it sees, and that it rarely confuses stages of AD with one another. Table VI also shows that there were no misclassifications. This could be due to the LR's ability to interpret key differences amongst the antenna measurements between the different cases.

Table VII shows the classification report that lists the precision, recall, F1-score, and support score for each of the class after the validation dataset was passed to the LR algorithm. It was found that LR had an overall accuracy of 100% on the validation dataset, which was expected due to its high performance on the training dataset. Precision is defined as the percent of predictions that were correct. It can be seen that all cases had a precision of 100%, as all the predictions were correct based on the data provided. Recall, which is the percentage of positive cases that were found by the ML classifier, was again 100% for all the cases.

TABLE VI
CONFUSION MATRIX FOR LR ALGORITHM

	Normal	Mild AD	Moderate AD	Severe AD
Normal	2	0	0	0
Mild AD	0	2	0	0
Moderate AD	0	0	2	0
Severe AD	0	0	0	2

TABLE VII
CLASSIFICATION REPORT FOR LR ALGORITHM ON VALIDATION DATASET

	Precision (%)	Recall (%)	F1 Scores (%)	Support (#)
Normal	1	1	1	2
Mild AD	1	1	1	2
Moderate AD	1	1	1	2
Severe AD	1	1	1	2

The F1 score is a weighted harmonic mean of precision and recall that determines the percent of positive predictions that are correct, which was 100%. Support, which is the actual number of points for each class in the dataset, sheds light on the number of datapoints for each class (i.e. stage of AD) that was present in the dataset.

C. *Method Limitations and Comparisons*

Table VIII shows the comparison of the LR model's accuracy in this paper along with the other RF-ML models that were used for microwave head imaging as described in [15]-[17]. It can be seen that the LR model used in this paper has a high accuracy score, but a much lower number of observations compared to other studies. This is due to the limited number of voxel models available in CST Microwave Studio Suite. However, these voxel models can be easily modified such that they can represent more cases. As a result, we plan to take advantage of this in order to create more cases and observations. In comparison, the SVM and LDA methods reported in [16] had the best accuracy and large number of observations. However, the methods used in [16] were applied for stroke detection, which contains a larger difference in dielectric properties as compared to the differences found in AD. As a result, the captured S_{11} measurements would reflect changes in the tissues more easily, and therefore allow the ML models to be trained easily. All the models had fast learning and classification times that could train their models and generate results in under a minute.

While the high accuracy is promising for the LR model in this paper, the small number of observations serves as a limitation of our method. Having a larger number of observations would enhance the analysis of the proposed method and allow us to determine how well the LR method is in classifying AD. Nonetheless, the very high accuracy score is a promising incentive of investigating this model further with a larger dataset of AD patients.

TABLE VIII
COMPARISON OF LR MODEL WITH OTHER RF-ML MODELS

Classifier	Accuracy (%)	Observations
SVM [15]	82.7	980
SVM [16]	99	180
LDA [16]	99	180
GDMI-SVM [17]	89	300
LR (This paper)	98.97	36

IV. CONCLUSION

This study investigated whether stages of AD could be classified with ML algorithms that were trained using RF data that noninvasively captured measurements of dielectric changes in the brain. Results indicate that LR is an accurate and efficient ML model that can be used for RF sensing and classification of AD noninvasively. The results obtained here provides a transformative approach to AD diagnostics and monitoring systems where ML can be integrated with RF sensing systems to intelligently predict the stage of AD in the brain. As a next step, ML algorithms will be investigated and evaluated on a much larger number of simulation cases in order to validate its performance on a larger group.

This works serves as a foundation for future work in the investigation of ML and DL techniques to RF imaging. Future research will focus on investigating DL techniques to classify AD traits from image data generated from the authors' previous work in [19]. In addition, the authors also plan to utiluse ML to classify AD based on other physiological changes in the brain that can be detected by RF sensors [32], [33]. Depending on these results, the next and final goal is to combine the different studies together to develop an AI solution that will take the captured RF data and predict the progression rate of AD in a patient. This, in turn, will be used to determine the different treatment strategies to slow down its progression. This would lead to a transformative and effective solution for future systems and techniques for AD monitoring and treatment delivery.

REFERENCES

[1] Alzheimer's Association, "2020 Alzheimer's disease facts and figures," *Alzheimer's Dement.*, vol. 16, pp. 391-460, 2020.

[2] Alzheimer's Association, "The Impact of COVID-19 and the Global Pandemic on Alzheimer's Research, Long-Term Care and the Brain," Presented at Alzheimer's Assoc. Int'l Conf., 2020. [Online]. Available:https://www.alz.org/aaic/releases_2020/covid-19-cognition-media-panel.asp.

[3] J. Escudero, E. Ifeachor, J. P. Zajicek, C. Green, J. Shearer, and S. Pearson, "Machine Learning-Based Method for Personalized and Cost-Effective Detection of Alzheimer's Disease," *IEEE Transactions on Biomedical Engineering*, vol. 60, no. 1, pp. 164-168, Jan. 2013.

[4] D. Holland, J. B. Brewer, D. J. Hagler, C. Fennema-Notestine, A.M. Dale, and the Alzheimer's Disease Neuroimaging Initiative, "Subregional neuroanatomical change as a biomarker for

Alzheimer's disease," in *Proc. Nat. Acad. Sci. U.S.A.*, vol. 106, no. 49, pp. 20954-20959, Dec. 2009.

[5] S. M. Landau, D. Harvey, C. M. Madison, R. A. Koeppe, E. M. Reiman, N. L. Foster, M. W. Weiner, and W. J. Jagust, "Associations between cognitive, functional, and FDG-PET measures of decline in AD and MCI," *Neurobiol. Aging*, vol. 32, no. 7, pp. 1207-1218, Jul. 2011.

[6] J. Q. Trojanowski, H. Vandeerstichele, M. Korecka, C. M. Clark, P. S. Aisen, R. C. Petersen, K. Blennow, H. Soares, et. al., "Update on biomarker core of the Alzheimer's Disease Neuroimaging Initiative subjects," *Alzheimer's Dement.*, vol. 7, no. 3, pp. 257-262, May 2011.

[7] S. Haller, D. Nguyen, C. Rodriguez, J. Emch, G. Gold, A. Bartsch, K. O. Lovblad, and P. Giannakopoulos, ``Individual prediction of cognitive decline in mild cognitive impairment using support vector machine based analysis of diffusion tensor imaging data," J. Alzheimer's Disease, vol. 22, no. 1, pp. 315-327, Sep. 2010.

[8] S. Al-Shoukry, T. H. Rassem and N. M. Makbol, "Alzheimer's Diseases Detection by Using Deep Learning Algorithms: A Mini-Review," in *IEEE Access*, vol. 8, pp. 77131-77141, 2020.

[9] C. Saraiva, C. Praça, R. Ferreira, T. Santos, L. Ferreira, and L. Bernardino,"Nanoparticle-mediated brain drug delivery: Overcoming blood-brain barrier to treat neurodegenerative diseases," *J. Controlled Release*, vol. 235, pp. 34-47, Aug. 2016.

[10] E. C. Fear and M. A. Stuchly, "Microwave detection of breast cancer," in IEEE Transactions on Microwave Theory and Techniques, vol. 48, no. 11, pp. 1854-1863, Nov. 2000, doi: 10.1109/22.883862.

[11] M. Persson et al., "Microwave-Based Stroke Diagnosis Making Global Prehospital Thrombolytic Treatment Possible," in IEEE Transactions on Biomedical Engineering, vol. 61, no. 11, pp. 2806-2817, Nov. 2014, doi: 10.1109/TBME.2014.2330554.

[12] M. Manoufali, A. T. Mobashsher, B. Mohammed, K. Bialkowski, P. C. Mills and A. Abbosh, "Implantable Sensor for Detecting Changes in the Loss Tangent of Cerebrospinal Fluid," in IEEE Transactions on Biomedical Circuits and Systems, vol. 14, no. 3, pp. 452-462, June 2020, doi: 10.1109/TBCAS.2020.2973387.

[13] J. Saluja, J. Casanova and J. Lin, "A Supervised Machine Learning Algorithm for Heart-Rate Detection Using Doppler Motion-Sensing Radar," in IEEE Journal of Electromagnetics, RF and Microwaves in Medicine and Biology, vol. 4, no. 1, pp. 45-51, March 2020, doi: 10.1109/JERM.2019.2923673.

[14] A. Santorelli, Y. Li, E. Porter, M. Popović and M. Coates, "Investigation of classification algorithms for a prototype microwave breast cancer monitor," The 8th European Conference on Antennas and Propagation (EuCAP 2014), The Hague, Netherlands, 2014, pp. 320-324, doi: 10.1109/EuCAP.2014.6901757.

[15] Y. Wu, M. Zhu, D. Li, Y. Zhang and Y. Wang, "Brain stroke localization by using microwave-based signal classification," 2016 International Conference on Electromagnetics in Advanced Applications (ICEAA), Cairns, QLD, Australia, 2016, pp. 828-831, doi: 10.1109/ICEAA.2016.7731527.

[16] T. Pokorny and J. Tesarik, "Microwave Stroke Detection and Classification Using Different Methods from MATLAB's Classification Learner Toolbox," 2019 European Microwave Conference in Central Europe (EuMCE), Prague, Czech Republic, 2019, pp. 500-503.

[17] G. Zhu, A. Bialkowski, L. Guo, B. Mohammed and A. Abbosh, "Stroke Classification in Simulated Electromagnetic Imaging Using Graph Approaches," in IEEE Journal of Electromagnetics, RF and Microwaves in Medicine and Biology, vol. 5, no. 1, pp. 46-53, March 2021, doi: 10.1109/JERM.2020.2995329.

[18] I. Saied, T. Arslan, S. Chandran, C. Smith, T. Spires-Jones and S. Pal, "Non-Invasive RF Technique for Detecting Different Stages of Alzheimer's Disease and Imaging Beta-Amyloid Plaques and Tau Tangles in the Brain," in *IEEE Transactions on Medical Imaging*, 2020.

[19] I. Saied, M. S. R. Bashri, T. Arslan, C. Smith and S. Chandran, "Dielectric Measurements of Brain Tissues with Alzheimer's Disease Pathology in the Microwave Region," *2019 IEEE International Symposium on Medical Measurements and Applications (MeMeA)*, Istanbul, Turkey, 2019, pp. 1-6.

[20] H. Braak and E. Braak, "Neuropathological stageing of Alzheimer-related changes." *Acta Neuropathologica, vol. 82*, no. 4, 2015, pp. 239-259.

[21] A. Arayeshnia, A. Keshtkar and S. Amiri, "Realistic human head voxel model for brain microwave imaging," *2017 Iranian Conference on Electrical Engineering (ICEE)*, Tehran, 2017, pp. 1660-1663.

[22] Z. Erlangung, "Detailed modeling of the human body in motion to investigate the electromagnetic influence of fields in a realistic environment", Thesis, Technische Universitat Darmstadt, 2018.

[23] G. M. Noetscher et al., "Virtual Humans for antenna/implant modeling," 2017 IEEE International Symposium on Antennas and Propagation & USNC/URSI National Radio Science Meeting, 2017, pp. 223-224, doi: 10.1109/APUSNCURSINRSM.2017.8072154.

[24] Dr. T. Wittig, "Analyzing HF & LF RadHaz Scenarios with 3D EM Simulation," *CST Studio Suite Webinar Series* [Online], Accessed: May 25, 2021, Available: https://www.ieee.li/pdf/viewgraphs/analyzing_radhaz_scenarios_with_3d_em_simulation.pdf

[25] J. Brownlee, *Master Machine Learning Algorithms*, 2016.

[26] Y. A. Ghassabeh, F. Rudzicz, H. A. Moghaddam, "Fast incremental LDA feature extraction," *Pattern Recognition*, vol. 48, no. 6, pp. 1999–2012, 2015.

[27] T. Mitchell, *Machine Learning*, McGraw Hill, ch. 8, pp. 231-247, 1997

[28] S. Russell, P. Norvig, *Artificial Intelligence: A Modern Approach (2nd ed.)*, Prentice Hall. ISBN 978-0137903955, 2003.

[29] C. Cortes, and V. Vapnik, "Support-vector networks," *Mach. Learn.*, vol. 20, pp. 273–297, 1995.

[30] M. Kuhn and K. Johnson, *Applied Predictive Modeling*, Springer, ch. 4, pp. 70, 2013.

[31] G. James, D. Witten, T. Hastie, and R. Tibshirani, *An Introduction to Statistical Learning with Applications in R*, Springer, ch. 5, pp. 181-185, 2017.

[32] I. M. Saied and T. Arslan, "Noninvasive Wearable RF Device Towards Monitoring Brain Atrophy and Lateral Ventricle Enlargement," in IEEE Journal of Electromagnetics, RF and Microwaves in Medicine and Biology, vol. 4, no. 1, pp. 61-68, March 2020, doi: 10.1109/JERM.2019.2926163.

[33] I. M. Saied, S. Chandran and T. Arslan, "Integrated Flexible Hybrid Silicone-Textile Dual-Resonant Sensors and Switching Circuit for Wearable Neurodegeneration Monitoring Systems," in IEEE Transactions on Biomedical Circuits and Systems, vol. 13, no. 6, pp. 1304-1312, Dec. 2019, doi: 10.1109/TBCAS.2019.2951500.

Imran M. Saied obtained his B.Sc. degree in electrical engineering from the Georgia Institute of Technology, Atlanta, GA, USA, in 2009, M.Sc. degree in electrical engineering from California State University-Fullerton, Fullerton, CA, USA, in 2011, and Ph.D. degree with the University of Edinburgh, Edinburgh, UK, in 2021, where his research focused on investigating the use of RF and microwaves for monitoring and detecting neurodegenerative diseases.

Prior to beginning his Ph.D., Dr. Saied worked as a Research Assistant with the Petroleum Institute (now Khalifa University) in Abu Dhabi, U.A.E. from 2013 to 2017. He worked on developing several tomography and spectroscopy systems for real-time oil and gas pipeline monitoring systems. In particular, he focused on THz spectroscopy, ECT/ECAT tomography, and development of sensors and imaging algorithms for these systems. The results from his work have led to several refereed journal and conference papers that have been published in IEEE and SPE. Currently, he is a postdoctoral research fellow at the Advanced Care Research Centre in the University of Edinburgh.

Tughrul Arslan holds the Chair of Integrated Electronic Systems with the School of Engineering, University of Edinburgh, Edinburgh, U.K. He is a member of the Integrated Micro and Nano Systems (IMNS) Institute and leads the Embedded Mobile and Wireless Sensor Systems (Ewireless) Group with the University (ewireless.eng.ed.ac.uk). His research interests include developing low power radio frequency sensors for wearable and portable biomedical applications. He is the author of more than 500 refereed papers and inventor of more than 20 patents.

Prof. Arslan is currently an Associate Editor for the IEEE Transactions on VLSI Systems and was previously an Associate Editor for the IEEE Transactions on Circuits and Systems I (2005–2006) and IEEE Transactions on Circuits and Systems II (2008–2009). He is also a member of the IEEE CAS executive committee on VLSI Systems and Applications (1999 to date), and a member of the steering and technical committees of a number of international conferences. He is a co-founder of the NASA/ESA conference on Adaptive Hardware and Systems (AHS) and currently serves as a member of its steering committee.

Siddharthan Chandran holds the MacDonald Chair of Neurology with the Centre for Clinical Brain Sciences, University of Edinburgh, Edinburgh, U.K. He works in the emerging discipline of Regenerative Neurology. His research combines laboratory activity that includes human stem cells with specialist clinics to both study several neurodegenerative diseases as well as undertake early phase clinical trials. He is also the Director of the Anne Rowling Regenerative Neurology Clinic and Programme Lead of the UK Dementia Research Institute with the University of Edinburgh, where he leads and develops research activities and clinical experimental infrastructure for longitudinal studies.